Supporting Information

A Cryogenic Luminescent Ratiometric Thermometer Based on a Lanthanide Phosphonate Dimer

Min Ren,[a] Carlos D. S. Brites, [b] Song-Song Bao,[a] Rute A. S. Ferreira,[b] Li-Min Zheng[a] and Luis D. Carlos*[b]*

Min Ren, Dr. Song-Song Bao, Prof. Dr. Li-Min Zheng
State Key Laboratory of Coordination Chemistry, School of Chemistry and Chemical Engineering, Collaborative Innovation Center of Advanced Microstructures, Nanjing University, Nanjing 210093, China.
E-mail: lmzheng@nju.edu.cn

Dr. C. D. S. Brites, Prof. Dr. R. A. S. Ferreira, Prof. Dr. L. D. Carlos
Physics Department, CICECO - Aveiro Institute of Materials, University of Aveiro, 3810-193, Aveiro, Portugal
E-mail: lcarlos@ua.pt

Experimental Section

General: The ligand 1,4,7-triazacyclononane-1,4,7-triyl-tris(methylene phosphonic acid) ($notpH_6$) was prepared according to literature methods.[1] Compounds 1 and 2 were synthesized following the previously reported method.[2] All the other starting materials were of reagent grade quality and were obtained from commercial sources without further purification. Elemental analysis for C, H and N were carried out on a PE 240C analyzer. IR spectra were recorded with a TENSOR 27 Fourier transform infrared spectrophotometer. Thermal analyses were performed in nitrogen on a METTLER TOLEDO TGA instrument. Powder X-ray diffraction (PXRD) data were collected in a Bruker D8 advance diffractometer.

*Synthesis of $[Eu(notpH_4)(NO_3)(H_2O)]_2{\cdot}8H_2O$ (**1**).* A solution of $notpH_6$ (0.4 mmol, 160.6 mg) and $Eu(NO_3)_3{\cdot}6H_2O$ (1.2 mmol, 547.2 mg) in water (20 mL) was adjusted by addition of 1M HNO_3 to pH 1.33. After keeping at room temperature for 2 weeks, colorless parallelogrammic crystals of **1** were collected. Yield: 135.2 mg (24%, based on ligand). Elemental analysis calcd (%) for $C_{18}H_{48}N_8P_6O_{26}Eu_2{\cdot}8H_2O$: C 15.16, H 4.52, N 7.86; found C 14.42, H 4.81 N, 7.48. IR (KBr, cm^{-1}): 3526–2852 (br), 2360 (m), 1667 (m), 1384 (s), 1332 (m), 1158 (s), 1143 (s), 1064 (s), 995 (m), 932 (m), 775 (m), 556 (m). Thermal analysis shows that the weight loss in the 303−533 K range is 12.1%, close to the calculated value for the release of two coordinated and eight crystal water molecules (12.6%).

*Synthesis of $[Tb(notpH_4)(NO_3)(H_2O)]_2{\cdot}8H_2O$ (**2**).* Preparation of this compound follows the same procedure as for **1** except that $Tb(NO_3)_3{\cdot}6H_2O$ (1.2 mmol, 545.7 mg) was used as the starting material instead of $Eu(NO_3)_3{\cdot}6H_2O$. The clear solution was left at room temperature for 2 weeks to afford colorless parallelogrammic crystals in a yield of 90.8 mg (16% based on $notpH_6$). Elemental analysis calcd (%) for $C_{18}H_{48}N_8P_6O_{26}Tb_2{\cdot}8H_2O$: C 15.01, H 4.48, N 7.78; found: C 14.64, H 4.76, N 7.37. IR (KBr, cm^{-1}): 3519-2853 (br), 2390 (w), 1668 (m), 1384 (s), 1332 (m), 1158 (s), 1142 (s), 1066 (s), 993 (m), 933 (m), 748 (m), 556 (m), 487 (m). Thermal analysis

shows that the weight loss in the 303−533 K range is 12.3 %, close to the calculated value for the release of two coordinated and eight crystal water molecules (12.5%).

*Synthesis of $[Eu_{0.102}Tb_{0.898}(notpH_4)(NO_3)(H_2O)]_2{\cdot}8H_2O$ (**3**).* A mixture of 23.76 mL 0.05 M $Tb(NO_3)_3$ solution and 0.12 mL 0.1 M $Eu(NO_3)_3$ solution was added into the solution of $notpH_6$ (0.4 mmol, 160.6 mg) in water (15 mL), adjusted pH to 1.34 by addition of 1M HNO_3. The clear solution was left at room temperature for 2 weeks to afford colorless prismatic crystals in a yield of 37% based on $notpH_6$. Elemental analysis calcd (%) for $C_{18}H_{48}N_8P_6O_{26}Tb_{1.796}Eu_{0.204}{\cdot}8H_2O$: C 15.02, H 4.48, N 7.79; found: C 15.35, H 4.61, N 7.65. FTIR (KBr, cm^{-1}): 3520-2853 (br), 2359 (w), 1668 (m), 1384 (s), 1332 (m), 1158 (s), 1142 (s), 1066 (s), 993 (m), 933 (m), 749 (m), 557 (m), 487 (m). Thermal analysis shows that the weight loss in the 303-533 K range is 11.8 %, close to the calculated value for the release of two coordinated and eight crystal water molecules (12.5%).

Crystallographic analyses. Data collection was carried out on a Bruker SMART APEXII CCD diffractometer equipped with graphite monochromated MoK_α (λ = 0.071073 nm) radiation at 173(2) K. The data were integrated using the Siemens SAINT program,[3] with the intensities corrected for Lorentz factor, polarization, air absorption, and absorption due to variation in the path length through the detector faceplate. Empirical absorption and extinction corrections were applied. The structure was solved by direct method and refined on F^2 by full-matrix least squares using SHELXTL.[4] All the non-hydrogen atoms were refined anisotropically. All the hydrogen atoms were put in calculated positions or located from the Fourier maps and refined isotropically with the isotropic vibration parameters related to the non-hydrogen atom to which they are bonded.

Photoluminescence properties were investigated using a modular double grating excitation spectrofluorimeter with a TRIAX 320 emission monochromator (Fluorolog-3, Horiba Scientific) coupled to a R928 Hamamatsu photomultiplier, using a front face acquisition mode. The excitation source was a 450 W Xe arc lamp. The emission spectra were corrected for detection and optical spectral response of the spectrofluorimeter and the excitation spectra were corrected for the spectral

distribution of the lamp intensity using a photodiode reference detector. The time-resolved emission spectra and emission decay curves were acquired with the same instrumentation using a pulsed Xe–Hg lamp (6 μs pulse at half width and 20–30 μs tail).

Temperature Control. The temperature-dependent photoluminescence measurements were performed using a He closed-cycle cryostat, and the temperature (18−300 K, with a maximum accuracy of 0.1 K) was increased with a Lakeshore 331 auto-tuning temperature controller with a resistance heater.

Temperature calibration. The sample temperature was fixed to a particular value using the auto-tuning temperature controller; after waiting 5 minutes to thermalize the sample, the steady state emission spectrum of the samples was measured; the maximum temperature difference detected during the acquisitions was 0.1 K, the temperature accuracy of the controller; the emission spectrum was converted to temperature through the thermometric parameter Δ.

References:

[1] T. J. Atkins, J. E. Richman, W. F. Oettle, *Org. Synth.* 1978, 58, 87.

[2] S. S. Bao, L. F. Ma, Y. Wang, L. Fang, C. J. Zhu, Y. Z. Li, L. M. Zheng, *Chem-Eur. J.* 2007, 13, 2333.

[3] SAINT, *Program for Data Extraction and Reduction*, Siemens Analytical X-ray instruments, Madison, WI 1994-1996.

[4] SHELXTL, *Reference Manual (version 5)*, Siemens Industrial Automation Analytical Instruments, Madison, WI 1995.

Structural Characterization

Table S1. Crystallographic data for compounds **1** and **2**.

Compound	**1**	**2**
Formula	$C_{18}H_{64}Eu_2N_8O_{34}P_6$	$C_{18}H_{64}Tb_2N_8O_{34}P_6$
M	1426.51	1440.43
Temperature /K	173(2)	173(2)
Crystal system	monoclinic	monoclinic
Space group	$P2_1/c$	$P2_1/c$
a / Å	10.8792(11)	10.8448(8)
b / Å	13.1682(11)	13.1903(10)
c / Å	17.0596(18)	16.9763(15)
β / deg	108.570(4)	108.512(2)
Z	2	2
V / Å^3	2316.7(4)	2302.7(3)
D_c / g·cm^{-3}	2.045	2.077
F(000)	1432	1440
Goodness-of-fit on F^2	0.961	1.012
R_1, wR_2[a] [I>2σ(I)]	0.0437, 0.0552	0.0412, 0.0623
R_1, wR_2 (all data)	0.0874, 0.0609	0.0854, 0.0722
$(\Delta\rho)_{max}$, $(\Delta\rho)_{min}$/[e Å^{-3}]	0.765, -1.177	0.985, -1.082
CCDC number	1059019	1059020

[a] $R_1 = \sum \| F_0 | - | F_c \| / \sum | F_0 |$; $wR_2 = \left[\sum w \left(F_0^2 - F_C^2 \right)^2 / \sum w \left(F_C^2 \right)^2 \right]^{1/2}$

Table S2. Selected bond lengths (Å) for compounds **1** and **2**.

Compound	**1**	**2**		**1**	**2**
Ln1-O1	2.598(4)	2.585(4)	P1-O1	1.534(4)	1.532(4)
Ln1-O1W	2.411(5)	2.380(4)	P1-O2	1.513(4)	1.520(4)
Ln1-O2	2.417(4)	2.377(4)	P1-O3	1.509(5)	1.508(5)
Ln1-O4	2.484(4)	2.463(4)	P2-O4	1.534(5)	1.527(4)
Ln1-O7	2.361(3)	2.330(3)	P2-O5	1.566(5)	1.571(5)
Ln1-O10	2.717(4)	2.735(4)	P2-O6	1.505(4)	1.506(4)
Ln1-O11	2.515(4)	2.484(4)	P3-O7	1.492(4)	1.500(4)
Ln1-O1A	2.327(3)	2.301(3)	P3-O8	1.586(5)	1.581(4)
Ln1-O6A	2.454(4)	2.428(4)	P3-O9	1.505(5)	1.501(5)

Symmetry transformations used to generate equivalent atoms: A: 1-*x*, 2-*y*, 1-*z*

Table S3. Selected bond angles [degree, °] for compounds **1** and **2**.

Compound	**1**	**2**
O1-Ln1-O1W	141.28(12)	141.37(12)
O1-Ln1-O2	58.02(12)	58.47(12)
O1-Ln1-O4	70.67(14)	70.82(13)
O1-Ln1-O7	119.42(13)	119.88(13)
O1-Ln1-O10	126.71(13)	126.32(13)
O1-Ln1-O11	134.85(14)	135.00(14)
O1-Ln1-O1A	70.28(13)	70.16(13)
O1-Ln1-O6A	70.02(13)	70.08(13)
O1W-Ln1-O2	149.31(12)	149.01(12)
O1W-Ln1-O4	81.11(14)	81.22(14)
O1W-Ln1-O7	75.35(13)	75.07(13)
O1W-Ln1-O10	64.85(13)	64.76(13)
O1W-Ln1-O11	82.26(14)	81.99(14)
O1A-Ln1-O1W	79.62(13)	79.75(14)
O1W-Ln1-O6A	128.34(13)	128.22(14)
O2-Ln1-O4	89.26(14)	89.32(14)
O2-Ln1-O7	73.99(14)	73.97(14)
O2-Ln1-O10	129.43(13)	129.50(14)
O2-Ln1-O11	90.70(14)	90.48(14)
O1A-Ln1-O2	127.66(14)	127.99(14)
O2-Ln1-O6A	76.05(13)	76.13(13)
O4-Ln1-O7	74.30(15)	74.33(12)
O4-Ln1-O10	141.30(14)	141.17(14)
O4-Ln1-O11	147.00(15)	146.69(14)
O1A-Ln1-O4	80.69(15)	80.97(12)
O4-Ln1-O6A	140.03(14)	140.29(13)
O7-Ln1-O10	111.62(14)	111.63(14)
O7-Ln1-O11	74.00(14)	73.63(14)
O1A-Ln1-O7	146.85(15)	146.91(15)
O6A-Ln1-O7	133.24(13)	133.09(13)
O10-Ln1-O11	48.47(15)	48.88(15)
O1A-Ln1-O10	75.74(14)	75.29(14)
O6A-Ln1-O10	64.35(14)	64.21(14)
O1A-Ln1-O11	123.77(15)	123.74(15)
O6A-Ln1-O11	71.32(14)	71.33(14)
O1A-Ln1-O6A	79.66(13)	79.69(13)

Symmetry transformations used to generate equivalent atoms: A: $-x+1, -y, -z+1$; B: $-x, -y, -z+1$; C: $-x, -y+1, -z+1$

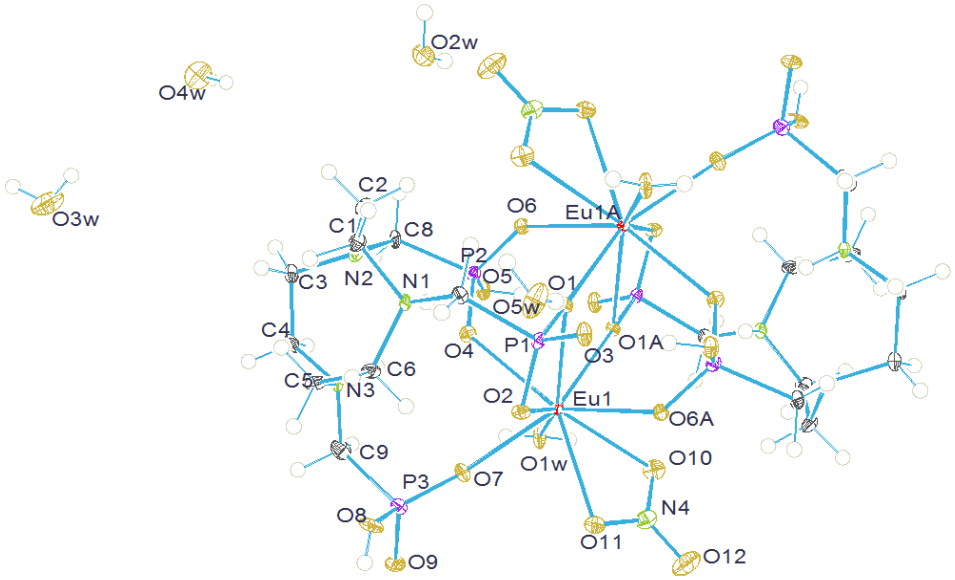

Figure S1 The molecular structure of compound **1** with atomic labeling scheme (50% probability). Symmetry code: A: –*x*+1, –*y*, –*z*.

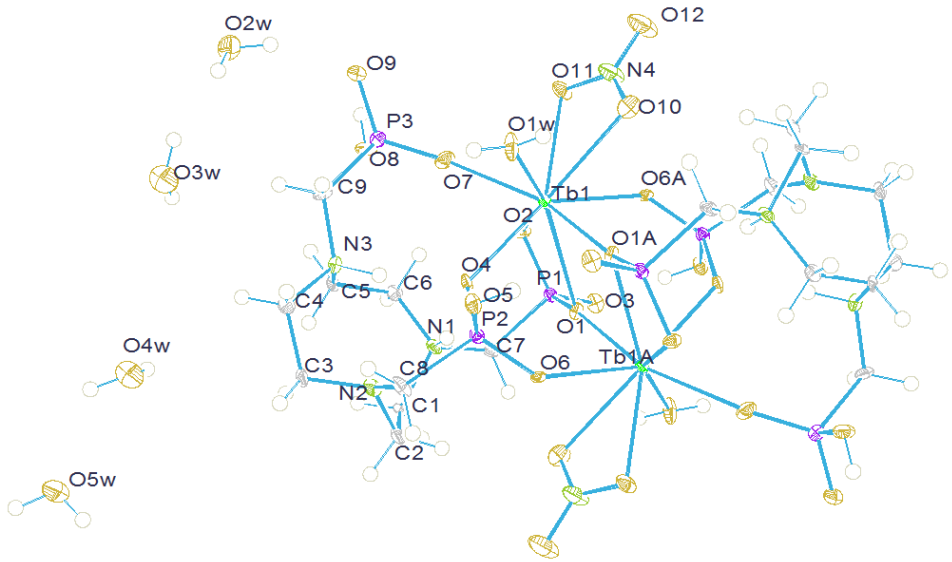

Figure S2 Molecular structure of compound **2** with atomic labeling scheme (50% probability). Symmetry code: A: –*x*+1, –*y*, –*z*.

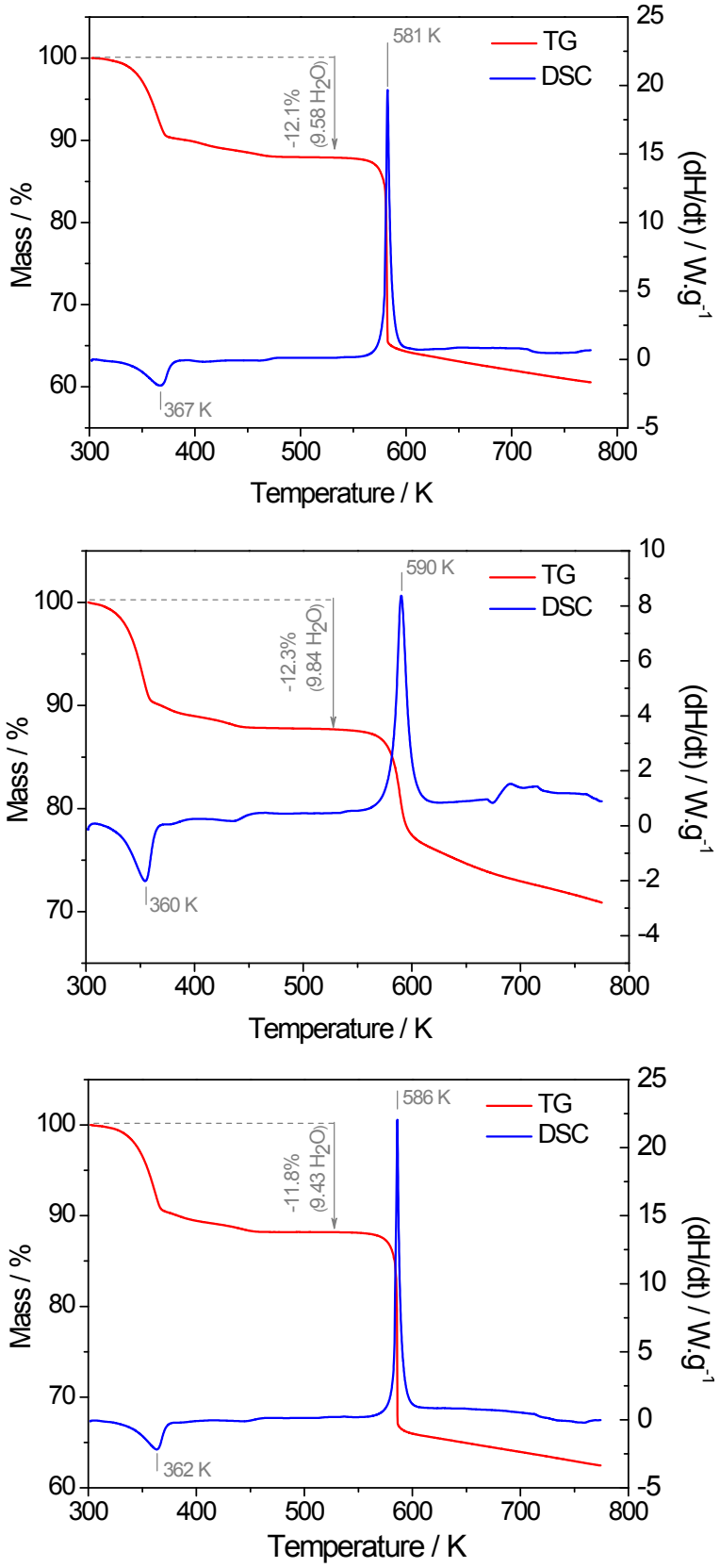

Figure S3. TG analyses of compounds **1** (top), **2** (middle) and **3** (bottom).

Photoluminescence and PXRD

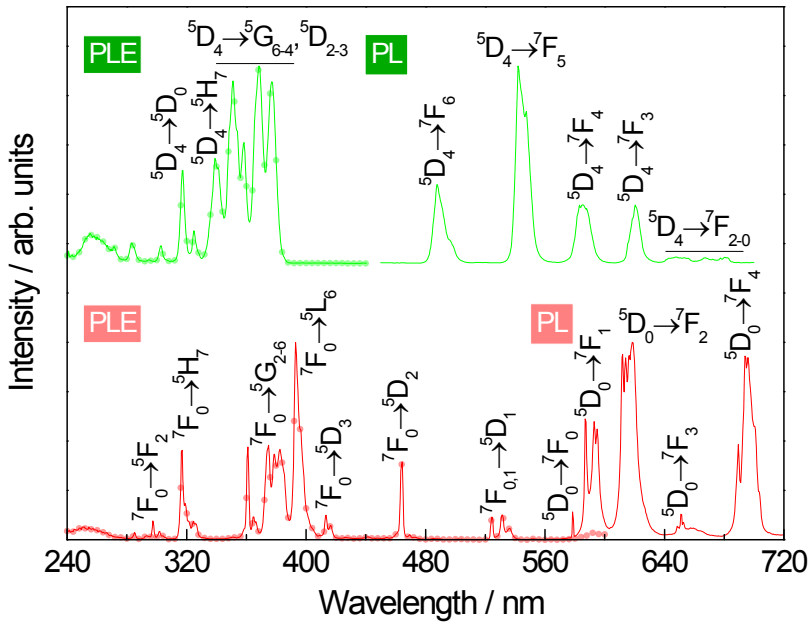

Figure S4. Room-temperature excitation (PLE, solid lines with circles) monitored at 619 nm (**1**) and 542 nm (**2**) and emission (PL, solid lines) spectra of **1** (red) and **2** (green) excited at 395 and 377 nm, respectively.

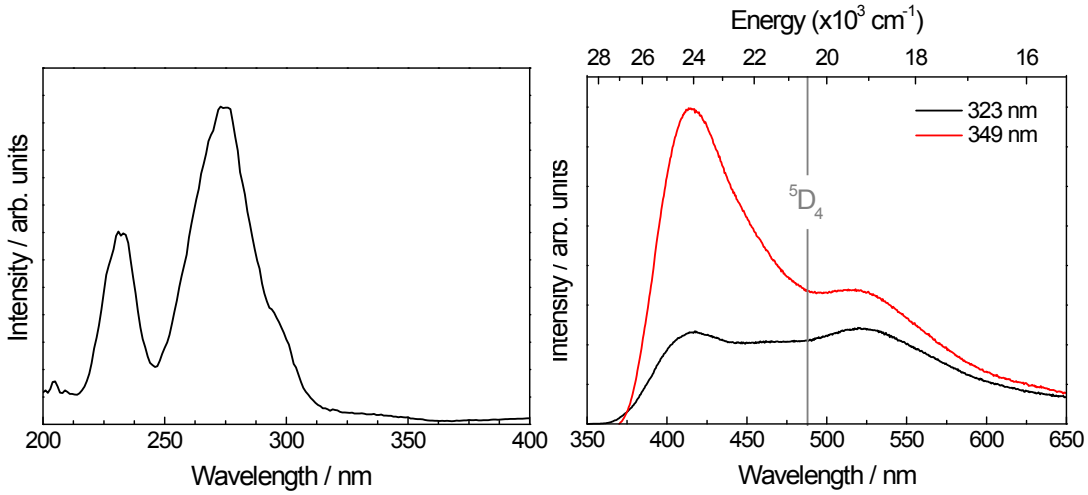

Figure S5. (left) Diffuse reflectance and (right) emission spectra excited at 323 and 349 nm of the notpH$_6$ ligand. The vertical line assigns thebarycenter position of the $^5D_4$ (Tb^{3+}) level.

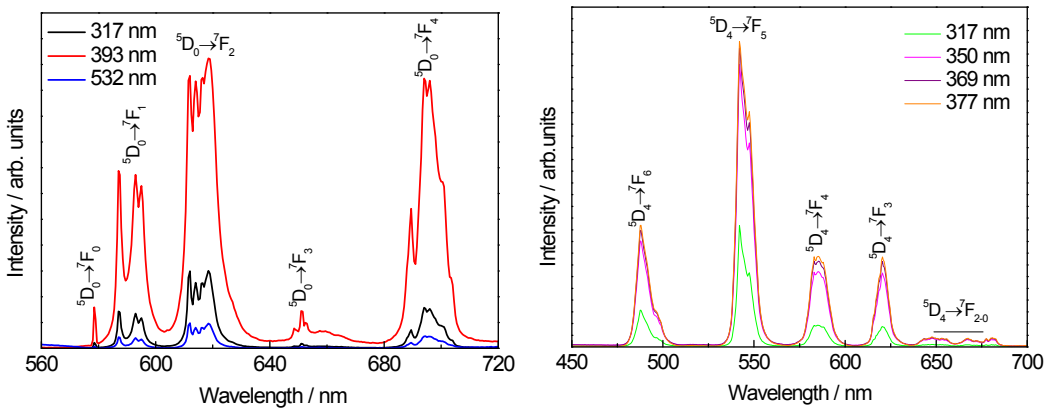

Figure S6. Room-temperature emission spectra of compounds **1** (left) and **2** (right) as a function of the excitation wavelength.

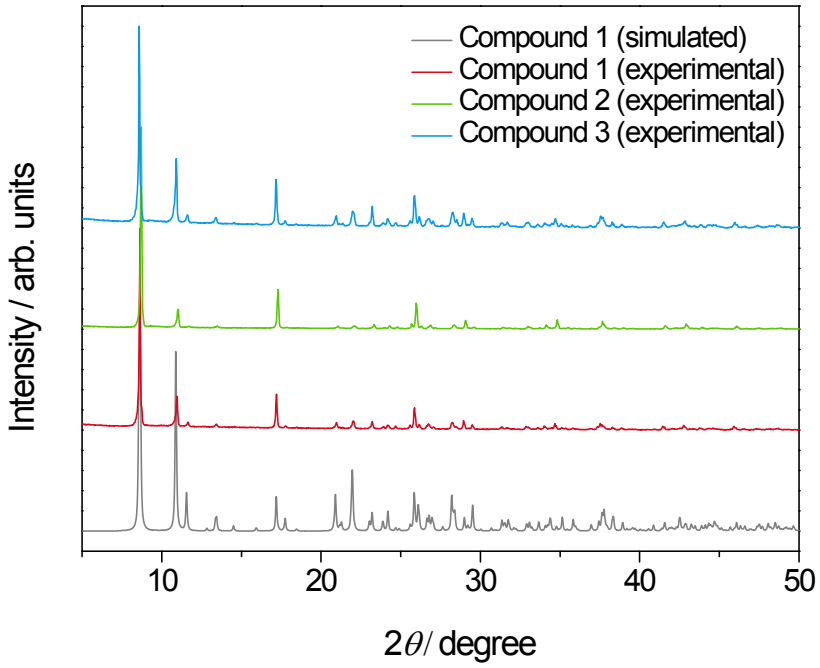

Figure S7. PXRD patterns for compounds **1-3** and that simulated from the single crystal data of compound **1**.

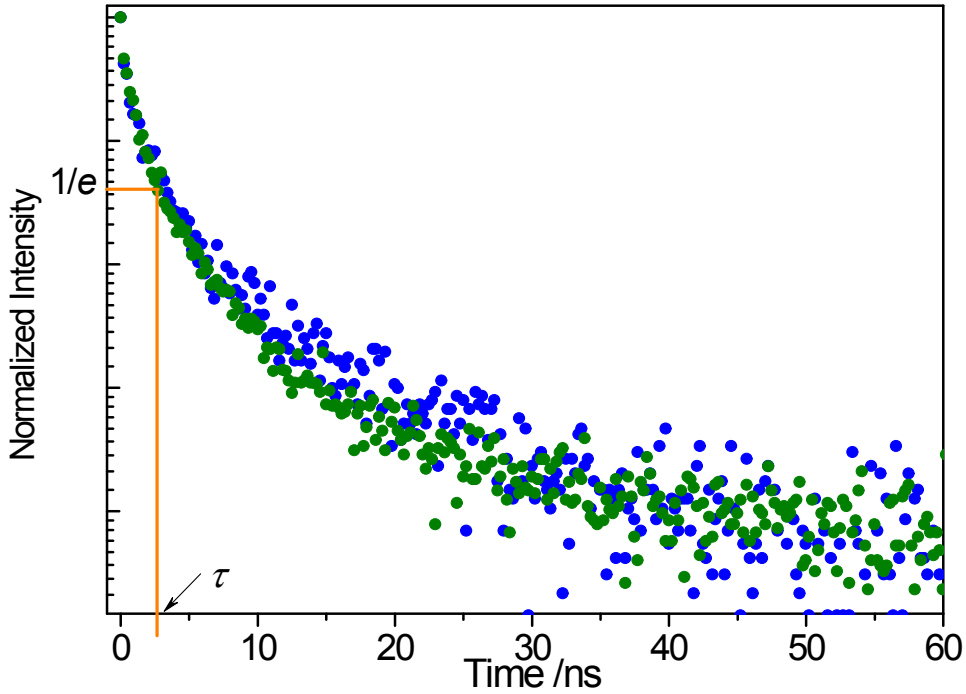

Figure S8. Emission decay curves of the notpH$_6$ ligand excited at 355 nm and monitored at 415 (blue) and 525 nm (green). The emission decay curve of the notpH$_6$ ligand reveals a non-exponential behavior with an average lifetime value (defined as the time at which the initial intensity is decreased by *1/e*) $\tau = 2.5 \pm 0.1 \times 10^{-9}$ s.

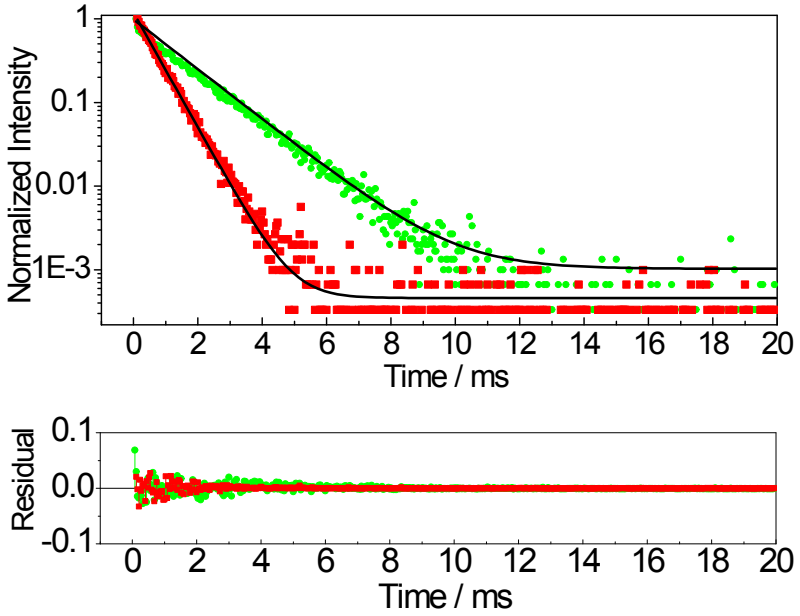

Figure S9. Emission decay curves of **1** monitored at 619 nm and excited at 393 nm (red) and of **2** monitored at 542 nm and excited at 377nm (green). The solid lines represent the data best fit (r^2>0.980) using a single exponential function. The residual plots are also shown (bottom).

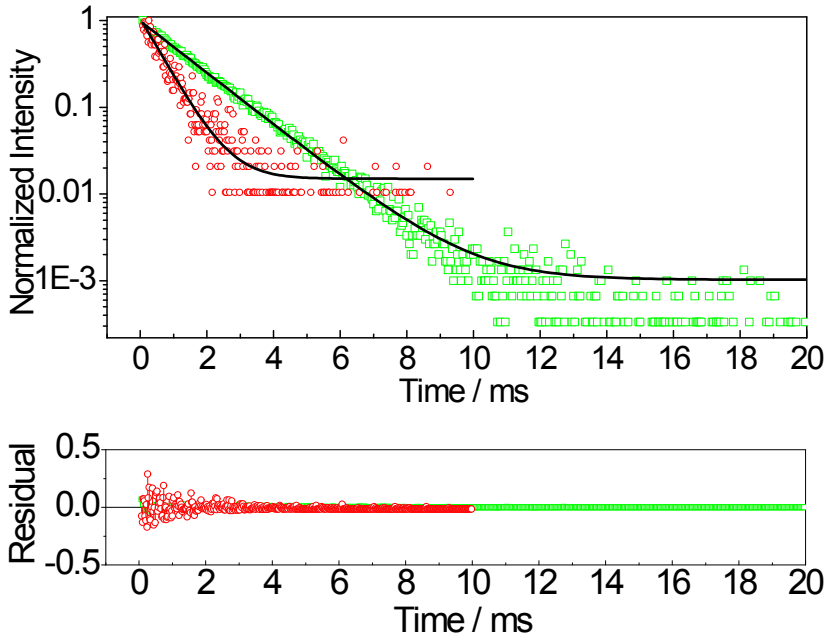

Figure S10. Emission decay curves of **3** monitored at 619 nm and excited at 393 nm (red) and monitored at 542 nm and excited at 377nm (green). The solid lines represent the data best fit (r^2>0.980) using a single exponential function. The residual plots are also shown (bottom).

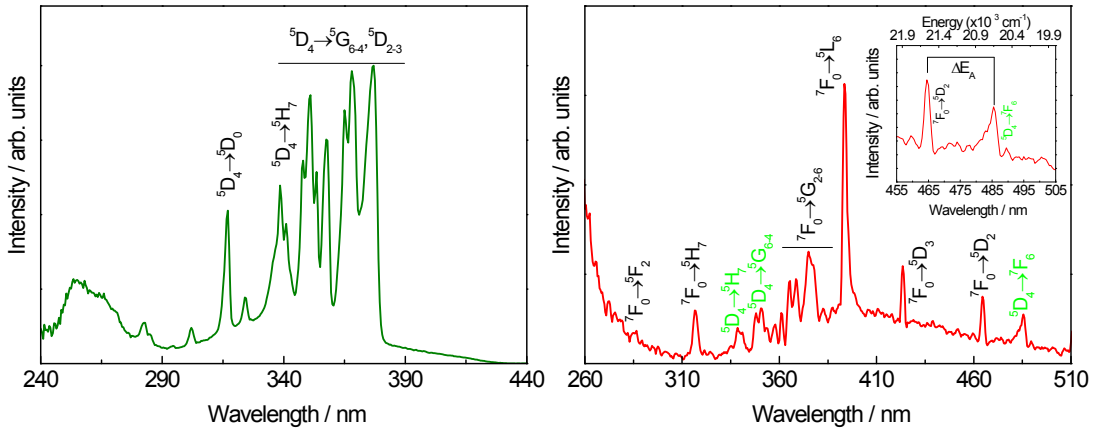

Figure S11. Excitation spectra (18 K) for compound **3** monitored at 542 nm (left) and at 696 nm (right). The inset shows a magnification in the 455−505 nm region.

Details on the Mott-Seitz model used

Mott described the total transition probability of an emitting level by the sum of radiative and non-radiative transition probabilities (W_R and W_{NR}, respectively). This can be evaluated by the inverse of the lifetime of the emitting level using the classical Mott–Seitzmodel:[1-3]

$$\frac{1}{\tau(T)} = \frac{1}{\tau_R} + \frac{1}{\tau_{NR}}, \qquad \text{(Eq. S1)}$$

where τ_R is the radiative lifetime (assumed to be temperature independent and equal to τ_0) and τ_{NR} is the non-radiative lifetime that is described by the Arrhenius dependence: $\tau_{NR} = \tau_{NR}(0)\exp(-\Delta E / k_B T)$, where $\tau_{NR}(0)$, ΔE and k_B stand for the non-radiative decay time at T=0 K, the activation energy for the thermal quenching process and the Boltzmann constant, respectively. Solving Eq. S1 for the total (experimentally measured) lifetime one can write:

$$\tau(T) = \frac{\tau_0}{1 + \alpha \exp(-\Delta E / k_B T)} \qquad \text{(Eq. S2)}$$

where $\alpha = W_{NR}/W_R$ was introduced. When two quenching processes (A,B) are present the above expression should include the deactivation though these channels as:

$$\tau(T) = \frac{\tau_0}{1 + \alpha_A \exp(-\Delta E_A / k_B T) + \alpha_B \exp(-\Delta E_B / k_B T)} \qquad \text{(Eq. S3)}$$

The integrated luminescence intensity, $I(T)$, may be related with $\tau(T)$ as:

$$\frac{I(T)}{I_0} = \frac{\tau(T)}{\tau_0} \qquad \text{(Eq. S4)}$$

where I_0 is the beam intensity at T=0 K. From Eqs. S3 and S4 it follows:

$$I(T) = \frac{I_0}{1 + \alpha_A \exp(-\Delta E_A / k_B T) + \alpha_B \exp(-\Delta E_B / k_B T)} . \quad \text{(Eq. S5)}$$

Because the Δ ratiometric parameter is defined as the I_1/I_2 intensities ratio, the general dependence of $\Delta(T)$ is given by:

$$\Delta(T) = \frac{I_{01}}{1 + \alpha_{1A} \exp(-\Delta E_{1A} / k_B T) + \alpha_{1B} \exp(-\Delta E_{1B} / k_B T)} \times \frac{1 + \alpha_{2A} \exp(-\Delta E_{2A} / k_B T) + \alpha_{2B} \exp(-\Delta E_{2B} / k_B T)}{I_{02}} \quad \text{(Eq. S6)}$$

where, $\alpha_{1,2\ A}$, $\alpha_{1,2\ B}$, stands for the ratio between the non-radiative and radiative probabilities of channels A and B, $\Delta E_{1,2\ A}$, $\Delta E_{1,2\ B}$ for the activation energy of channels A and B and $I_{01,2}$ for the integrated intensity at $T = 0$ K, all for the transitions 1 (Tb^{3+}) and 2 (Eu^{3+}), respectively.

In this work, however, we observe that the deactivation of the Eu^{3+} transition is negligible compared to the Tb^{3+}one, which is equivalent to consider that $\alpha_{2A} \exp(-\Delta E_{2A} / k_B T) + \alpha_{2B} \exp(-\Delta E_{2B} / k_B T) << 1$, resulting in the approximated expression:

$$\Delta(T) \approx \frac{\Delta_0}{1 + \alpha_A \exp(-\Delta E_A / k_B T) + \alpha_B \exp(-\Delta E_B / k_B T)} \quad \text{(Eq. S7)}$$

where $\Delta_0 = I_{01}/I_{02}$. To validate this assumption we perform the fit of experimental $I_1(T)$ and $\Delta(T)$ (Figure S12), resulting in the same fitting parameters for α and ΔE, within the fitting errors (Table S4).

References:

[1] N. F. Mott, Proc. Roy. Soc. 1938, 167, 0384.

[2] F. Seitz, T. Faraday Soc. 1939, 35, 0074.

[3] Z. Wang, D. Ananias, A. Carné-Sánchez, C. D. S. Brites, D. Maspoch, J. Rocha, L. D. Carlos, Adv. Funct. Mater. 2015, 10.1002/adfm.201500518.

Table S4. Fitting results of I_1(T) and $\Delta(T)$ to Eq. S5 and Eq. S7, respectively. The experimental data and fitting curves are represented in Figure S12.

Parameter fitted	**Equation**	α_A	ΔE_A/cm^{-1}	α_B	ΔE_B/cm^{-1}	r^2
I_1(T)	*S5*	2695±175	648±21	6.12±0.72	106.6±7.3	0.993
$\Delta(T)$	*S7*	2702 ± 204	650 ± 25	6.16 ± 0.57	106.6 ± 8.5	0.993

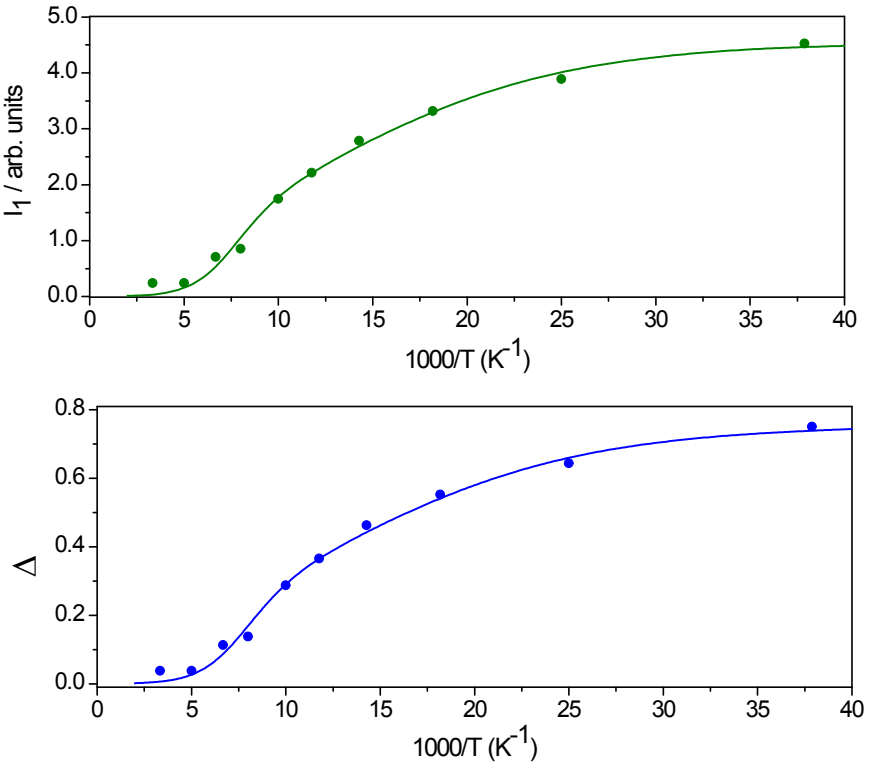

Figure S12 Arrhenius plots of I_1 (top) and Δ parameter (bottom) for the compound **3**. The solid lines are the best fit according to the classical Mott-Seitz model involving two non-radiative recombination channels. The fitting parameters are presented in Table S5.